JOURNAL OF SOLID STATE CHEMISTRY 51, 345–354 (1984)

Antimony-Doped Tin(IV) Oxide: Surface Composition and Electronic Structure

R. G. EGDELL,* W. R. FLAVELL, AND P. TAVENER

Inorganic Chemistry Laboratory, South Parks Road, Oxford OX1 3QR, United Kingdom

Received June 24, 1983; in revised form September 30, 1983

Antimony-doped tin(IV) oxide $Sn_{1-x}Sb_xO_2$ prepared by a high-temperature (1300 K) solid-state synthetic procedure has been studied over the composition range $0 < x < 0.03$ by X-ray and ultraviolet photoelectron spectroscopy (XPS and UPS) and high-resolution electron-energy-loss spectroscopy (HREELS). Pronounced enrichment by antimony close to the surface is evident from XPS with a heat of segregation approaching 30 kJ/mole. However, no increase in the surface free-carrier concentration is evident from the conduction-to-valence band intensity ratio in UPS or from the surface plasmon frequency in EELS. It is concluded that electrons associated with segregated Sb ions occupy a lone-pair-like *sp* hybrid surface state whose energy lies well below that of the conduction band.

1. Introduction

Ternary oxide systems find frequent application in catalysis, the flexibility of composition providing a means of improving efficiency and selectivity for "target" chemical reactions. In particular many technologically important selective oxidation catalysts are oxide materials containing two or more metal cations (*1*). It is widely recognized that the surface chemical composition important to catalytic activity may differ from that of the bulk and indeed atypical surface compositions have been demonstrated by the surface-sensitive technique of X-ray photoelectron spectroscopy in systems such as Bi–Mo–O (*2*) and Sn–Sb–O (*3*). However, little attention has been focused on the influence of segregation on the *electronic* structure of the material at the surface. In the present paper we use the complementary techniques of X-ray and ultraviolet photoelectron spectroscopy (XPS and UPS) and high-resolution electron-energy-loss spectroscopy (HREELS) both to monitor antimony segregation at the surface of doped tin(IV) oxide and to explore its impact on surface electronic structure.

Mixed oxides of tin and antimony have been developed as selective catalysts for the oxidation and ammoxidation of alkenes, notably propylene to acrolein and acrylonitrile. Optimal catalytic activity is obtained with fairly large antimony concentrations (~30% Sb cations (*4*), but the solubility limit of Sb in the rutile phase of SnO_2 is restricted to around 3 cation %. Calcination of mixtures with higher antimony content at 1000°C in air leads to loss of Sb_2O_4 and

* To whom correspondence and proofs should be addressed: Department of Chemistry, Imperial College of Science and Technology, South Kensington, London SW7 2AY, United Kingdom.

0022-4596/84 $3.00

eventually to formation of Sb-doped SnO_2 with limiting composition $Sn_{0.97}Sb_{0.03}O_2$. This material has been previously studied by Mössbauer spectroscopy which indicates the presence of bulk Sb(V) ions in a roughly octahedral environment, together with Sb(III) presumed to be at surface or grain boundary sites where the field gradient is large enough to produce incipient quadrupole splitting of the Mössbauer resonance (*5*). Segregation of antimony to surface and twin sites has also been discussed in relation to visible (*6*) and electron microscopy (*7*) of tin–antimony-oxide catalysts.

As emphasized in a recent review, the solid-state properties of the rutile phase $Sn_{1-x}Sb_xO_2$ are far from well understood (*4*): there is, for example, no general agreement as to the origin of the distinctive blue color found for compositions with $x > 0.005$ prepared by high-temperature reaction. In recent publications (*8, 9*) we have shown that electrons introduced by doping in $Sn_{0.97}Sb_{0.03}O_2$ occupy a free-electron-like conduction band and that the free-carrier concentration near the surface is close to its bulk value, despite dramatic surface enrichment by antimony. In the present paper we extend the results of the previous work with a study of $Sn_{1-x}Sb_xO_2$ embracing the complete composition range of the doped rutile phase ($0 < x < 0.03$). Although it is not generally agreed that the materials we have studied display optimal catalytic activity we believe that the insight into the electronic properties of this system provided by our experiments will be of value in developing understanding of the catalytic behavior.

2. Experimental

Samples were prepared by a coprecipitation method. Weighed quantities of Sn and Sb lumps (Koch Light, purity 99.999%) were dissolved in aqua regia made from BDH Analar grade acids. The solution was made alkaline with excess NH_3 and, after boiling for 2 hr, the resulting precipitate was collected and washed. After it was dried overnight at 420 K, the powdered material was finely ground in an agate mortar and fired for at least 14 days in air at 1300 K in a recrystallized alumina crucible, with occasional regrindings.

X-Ray powder diffractometry indicated the presence of a single well-crystallized rutile phase for each sample, with lattice parameters not significantly different from those of SnO_2 itself. Mean antimony contents of doped samples were found by atomic absorption spectroscopy to be close to nominal values. Examination of samples of $Sn_{0.97}Sb_{0.03}O_2$ in a 100-keV JEOL 100CX TEMSCAN analytical electron microscope revealed the presence of a single phase: Sn$K\alpha$ and Sb$K\alpha$ emissions indicated a homogeneous distribution of antimony with a mean antimony content equal to the bulk value. Our findings thus concur with those of Smith *et al.* (*7*) who used a 600-keV electron microscope to demonstrate that $Sn_{0.96}Sb_{0.04}O_2$ prepared by a method similar to that adopted here consisted predominantly of a well-crystallized rutile phase. Nominal compositions are used throughout the present work.

Prior to introduction into the electron spectrometer samples were pressed into pellets between optically smooth tungsten carbide dies and were then sintered for at least 24 hr in air at 1300 K to yield strong ceramic disks. Spectra were measured in an ESCALAB spectrometer (VG Scientific, East Grinstead, U.K.) with facilities for excitation of photoelectron spectra with unmonochromatized Al$K\alpha$ or Mg$K\alpha$ X rays or uv radiation from a noble-gas discharge lamp, as well as with a monochromatic electron source for HREELS. Samples mounted in platinum trays were cleaned in the preparation chamber of the spectrometer (base pressure 10^{-10} Torr) by annealing

at 820 K for at least 12 hr. They were then quenched to room temperature by rapid transfer from the heater stub to the "railway track," a large thermal capacity metal device that moves the sample from preparation to analysis chambers.

Surface cleanliness was monitored by HREEL spectra which under vacuo of around 10^{-10} Torr remained free of loss signals due to hydrocarbon or other contamination for periods of several hours. Electron spectra were accumulated in an ORTEC 620B multichannel analyzer and were transferred to floppy disks for subsequent analysis in a Research Machines Ltd. 380Z microcomputer.

3. Results and Discussion

3.1. Ultraviolet Photoelectron Spectra

Ultraviolet photoelectron spectra excited with He(I) ($h\nu$ = 21.2 eV) radiation are shown in Fig. 1. The spectra are in each case dominated by the full oxygen 2*p* valence band which has a sharp onset about 4 eV below the Fermi energy and merges with a strong and highly structured background of secondary electron emission beyond 10 eV. It is noteworthy that doping with antimony appears to have little effect on the valence band, which retains the shape characteristic of the undoped rutile phase of SnO_2. The overall O:2*p* bandwidth cannot be deduced from He(I) photoelectron spectra, although as we have discussed previously a bandwidth of about 10 eV may be observed in He(II) spectra ($h\nu$ = 40.8 eV) (*9*), in agreement with KKR (*10*) and tight-binding band-structure (*11*) calculations. The large bandwidth arises mainly from strong Sn—O covalency (*11*).

Close to the Fermi energy one finds in the spectra of the doped samples a weak peak that is best defined after subtraction of structure due to He$I\beta$ ($h\nu$ = 23.09 eV) radiation from the raw spectra. This corresponds to conduction electrons introduced by antimony doping. Taking the conduction and valence bands to be defined by their respective high-binding-energy minima, one can estimate the ratios between the areas of conduction and valence bands for compositions with $x > 0.001$ (0.1% Sb). The ratios are plotted against the composition parameter in Fig. 2. It will be seen that a linear variation is found. This would be expected on very simple grounds from the bulk nominal concentration of the dopant antimony but must be considered remarkable in view of the abnormal surface chemical composition of the doped material (section 3.3).

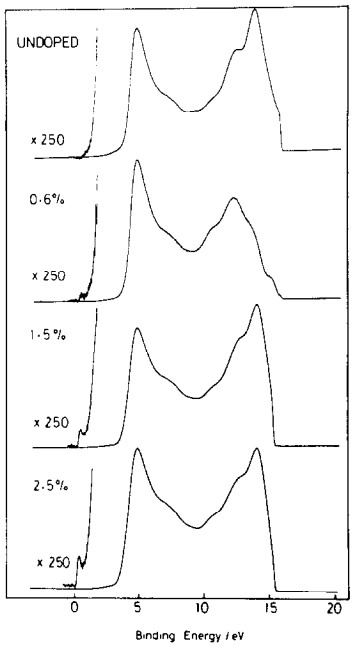

FIG. 1. He(I) photoelectron spectra of antimony-doped SnO_2 for various doping levels. He(I)β satellite structure has been subtracted from the spectra. Binding energies are relative to the Fermi energy E_F. The weak peak near E_F is due to conduction electrons introduced by the dopant.

It is interesting to consider the nature of the conduction band states in further detail. Transport measurements indicate that low concentrations of *n*-type dopants in SnO_2

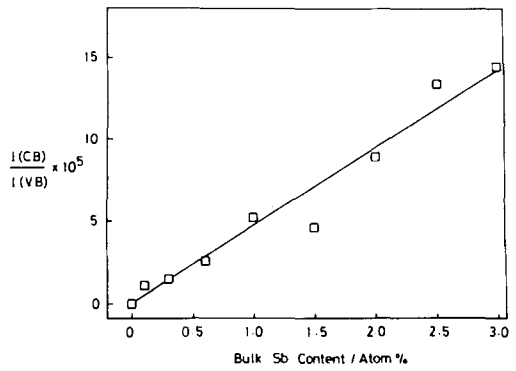

FIG. 2. Intensity ratio between conduction band (CB) and valence band (VB) in He(I) UPS of antimony-doped SnO_2.

give rise to a bound donor state $\Delta E_0 = 0.15$ eV below the conduction band minimum (*12*). The activation energy for conduction ΔE decreases with increasing donor concentration n according to an expression of the type:

$$\Delta E = \Delta E_0 - \alpha n^{1/3} \qquad (1)$$

where α is a constant. The critical carrier concentration n_c for $\Delta E = 0$ is 5.1×10^{18}/cm^3, corresponding to a value for the composition parameter $x = 1.8 \times 10^{-4}$ (0.018% Sb). From the well-established empirical correlation of Sienko and Edwards (*13*) a transition from nonmetallic to metallic behavior is to be expected when a modified Mott criterion is satisfied, i.e.,

$$n_c^{1/3} a_H^* = 0.26 \qquad (2)$$

where a_H^* is the effective donor radius given by:

$$a_H^* = a_H m_0 \varepsilon_\theta / m^* \qquad (3)$$

Here a_H is the Bohr-radius, m^*/m_0 is the electron effective mass ratio, and ε_θ is the static dielectric constant of the material under investigation.

From Eq. (2) we estimate an effective donor radius $a_H^* = 28.5 a_H$ at the donor concentration when $\Delta E = 0$ according to (1). This is close to the estimate $a_H^* = 22.9\ a_H$ obtained through Eq. (3), assuming a mean static dielectric constant $\varepsilon_\theta = 12.6$ consistent with the infrared reflectivity data of Summitt (*14*) and an effective mass ratio $m^*/m_0 = 0.55$ taken from our own HREELS data (section 3.2). Thus the disappearance of an activation energy for conduction at $n_c = 5.1 \times 10^{18}$/cm^3 may be interpreted as a semiconductor-to-metal transition conforming to the Edwards–Sienko criterion. Over the range of compositions where one may observe directly the conduction band in UPS ($x > 0.001$) Sb-doped SnO_2 is essentially a metallic material: the conduction electrons introduced by doping are not trapped at individual Sb ions but occupy the conduction band that is empty in pure SnO_2. Note, however, that metallic transport properties may not manifest themselves in measurements on polycrystalline material where the resistivity is dominated by grain boundary effects.

The tight binding calculations of Robertson indicate that the states at the bottom of the conduction band are of dominant (90%) Sn : 5*s* atomic character (*11*). It is thus possible to estimate the variation with x of the conduction-to-valence band intensity ratio $I(\mathrm{CB})/I(\mathrm{VB})$ using O : 2*p* and Sn : 5*s* atomic matrix elements for ionization from valence and conduction bands, respectively. From the calculations of Fadley and co-workers (*15*) one has the following one-electron ionization cross-sections: $\sigma(\mathrm{O}:2p) = 1.77$ Mb $\sigma(\mathrm{Sn}:5s) = 0.047$ Mb. Noting that there are twelve O : 2*p* electrons per formula unit we obtain

$$\frac{d(I(\mathrm{CB})/I(\mathrm{VB}))}{dx} = \frac{\sigma(\mathrm{Sn}:5s)}{12\sigma(\mathrm{O}:2p)} = 2.2 \times 10^{-3} \qquad (4)$$

Experimentally we have

$$\frac{d(I(\mathrm{CB})/I(\mathrm{VB}))}{dx} = 4.5 \times 10^{-3} \qquad (5)$$

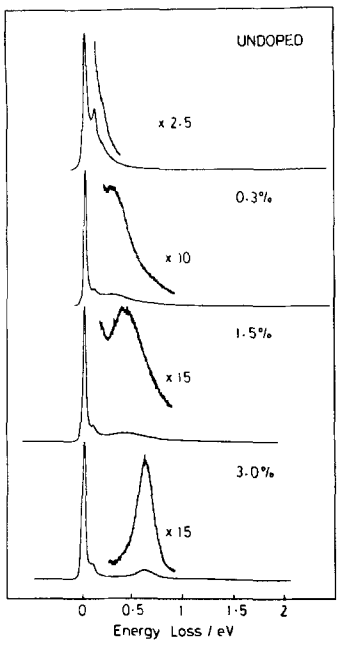

FIG. 3. Electron energy loss spectra of Sb-doped SnO_2 excited with a 25-eV electron beam. Instrumental resolution set at ~30 meV for these measurements.

The agreement between (4) and (5) is satisfactory in view of the simplicity of the theory used to define the intensity ratio in (4) and the fact that some of the more tightly bound valence band states are not observed in He(I) UPS. Thus our experiments confirm that UPS probes the bulk nominal conduction electron concentration over the composition range studied, and that the conduction band states are of predominant Sn : 5*s* atomic character.

3.2. *Electron Energy Loss Spectroscopy*

High-resolution electron energy loss spectra obtained with a 25-eV exciting electron beam are shown in Fig. 3. Close to the elastic peak one finds structure due to excitation of surface optical phonons, as discussed in detail elsewhere (*9*, *16*). However, the spectra of Fig. 3 are dominated by a fairly broad feature at $E_p = 0.59$ eV for $Sn_{0.97}Sb_{0.03}O_2$ that moves to progressively lower energy with decreasing antimony concentration. The variation in the energy of this loss feature shown in Fig. 4 is not linear with concentration: roughly speaking an $x^{1/2}$ dependence is found as shown in Fig. 5 where E_p^2 is plotted against x. This leads us to assign the loss peak to excitation of the conduction electron surface plasmon.

The loss function $P(\omega)$ for scattering of low energy electrons with velocity component v normal to the surface of a material with complex dielectric function $\varepsilon(\omega)$ is given by the expression (*17*):

$$P(\omega) = \frac{e^2}{v\hbar\omega} Im \frac{\varepsilon(\omega) - 1}{\varepsilon(\omega) + 1} \qquad (6)$$

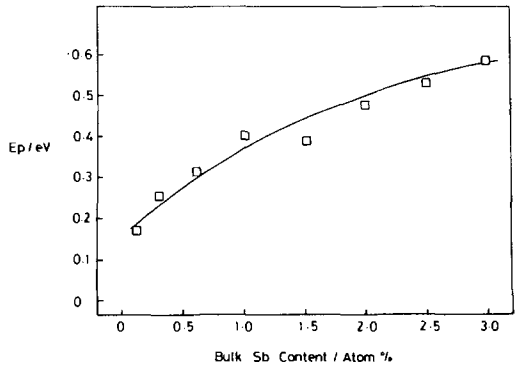

FIG. 4. Variation of plasmon energy E_P with Sb-doping level in $Sn_{1-x}Sb_xO_2$. The solid line is for heuristic purposes only. The error in E_P is ±0.02 eV.

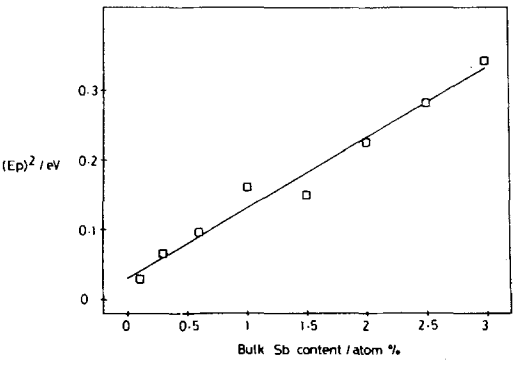

FIG. 5. Variation of square of plasma frequency with antimony doping in $Sn_{1-x}Sb_xO_2$. The solid line is a linear least-squares fit to the experimental data.

Peaks in the loss spectra thus correspond to the condition

$$Re(\varepsilon(\omega)) = -1 \tag{7}$$

Note that this loss condition differs from that for bulk losses for which:

$$Re(\varepsilon(\omega)) = 0 \tag{8}$$

For an array of damped oscillators with dynamic charge e, effective mass m^*, frequency ω_0, and damping constant γ one has

$$\varepsilon(\omega) = \varepsilon_\infty + \frac{ne^2}{m^* \varepsilon_0(\omega_0^2 - \omega^2 + i\omega\gamma)} \tag{9}$$

where n is the concentration of oscillators, ε_0 is the permittivity of free space, and ε_∞ is the background dielectric constant. Note that we have omitted the effect of local fields since we wish to deal with a metallic regime where local field corrections vanish (*18*). In the limit where $\omega_0 = 0$ Eq. (9) reduces to the familiar Drude dielectric function for a free-electron gas. From the observed loss frequencies in HREELS we have calculated electron effective masses through an expression derived from (8) and (9) that ignores damping, viz:

$$m^* = \frac{ne^2}{\varepsilon_0(\varepsilon_\infty + 1)(\omega_{sp}^2 - \omega_0^2)} \tag{10}$$

Where $\hbar\omega_{sp}$ is the observed surface plasmon loss energy and $\hbar\omega_0 = 0.15$ eV, the single-particle donor-level to conduction band excitation energy (*12*). We assume that the carrier concentration probed by HREELS is equal to the bulk nominal antimony doping levels. The effective mass ratios m^*/m_0 obtained in this way are given in Table I. It will be seen that the mass ratios show a fairly weak x-dependence with a wide scatter and are of the same order of magnitude as found in transport measurements (*19*). This provides justification for our analysis of the loss feature in terms of plasmon theory. Elsewhere we have shown that the effective mass from HREELS enables one to calculate the width and shape of the conduction band in UPS (*8*, *9*).

TABLE I

EFFECTIVE MASS OF CONDUCTION ELECTRONS IN Sb-DOPED SnO_2 FROM HREELS DATA

% Sb	Effective mass ratio m^*/m_0
0.3	0.55
0.6	0.65
1.0	0.60
1.5	0.90
2.0	0.80
2.5	0.60
3.0	0.75
$n_c = 1.75 \times 10^{17}/cm^3$	0.41[a]

[a] From transport measurements (Ref. (*19*)).

Some remarks about the optical properties of Sb-doped SnO_2 are warranted in view of our HREELS measurements. The blue color of such materials is probably due to a reflectivity minimum at the plasma frequency in the infrared, with a reflectivity that increases with increasing frequency through the visible region. This interpretation differs from the view that the blue color arises from Sb^{3+}–Sb^{5+} charge transfer excitation in the tin(IV) oxide matrix (*4*, *6*). In this context it is interesting to contrast our results for $Sn_{1-x}Sb_xO_2$ with those for formally related systems of the type $A_2Sn_{1-x}Sb_xCl_6$ studied by Atkinson and Day (*20*) (*A* being here a unipositive cation). In the latter materials blue coloration undoubtedly arises from a metal–metal charge-transfer absorption process, but the intervalence band shows little variation in energy with the level of doping. Thus in $(NH_4)_2Sn_{1-x}Sb_xCl_6$ the frequency shifts from 17,900 cm^{-1} at $x = 0.02$ to 19,200 cm^{-1} at $x = 0.28$. This variation is negligible compared with that found for the loss feature in the doped oxide system (Fig. 4) and compels one to recognize that differing excitation processes are involved.

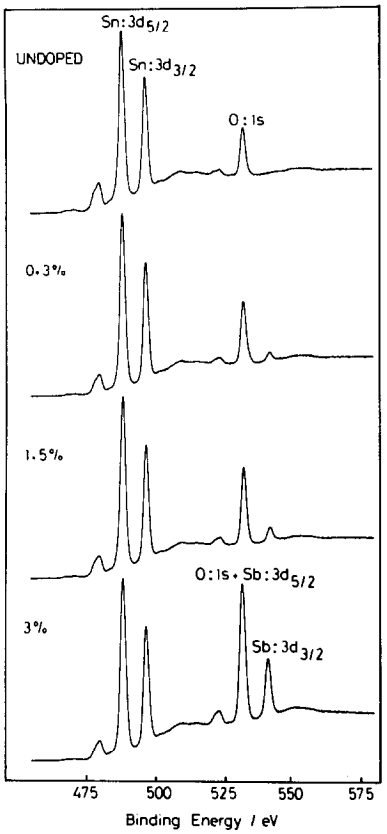

FIG. 6. Mg$K\alpha$ X-ray photoelectron spectra of $Sn_{1-x}Sb_xO_2$. Peaks to the left of the main features are due to satellite radiation.

3.3. X-Ray Photoelectron Spectra

Mg$K\alpha$ excited X-ray photoelectron spectra in the region of metal $3d$ ionizations are shown in Fig. 6. Unfortunately the Sb : $3d_{5/2}$ peak overlaps with the O : $1s$ peak but from the Sb : $3d_{3/2}$ intensity ratio it is evident that there is a pronounced surface enrichment in antimony for all compositions studied. This point is emphasized in Fig. 7 which shows that the intensity ratio $I(\mathrm{Sb}:3d_{3/2})/I(\mathrm{Sn}:3d_{3/2})$ does not correspond to the composition parameter x, and that there is a nonlinear variation with antimony-doping level.

In a previous publication (*9*) we showed that for $Sn_{0.97}Sb_{0.03}O_2$ the intensity ratio $I(\mathrm{Sb})/I(\mathrm{Sn})$ was higher for the $3d$ peaks than for the $4d$ peaks, where the photoelectron energy is substantially higher. Similar behavior was found for the materials with lower antimony content studied in the present work. Qualitatively this result shows that antimony enrichment is restricted to a surface "layer" thin compared with the electron mean free path, while quantitative analysis of the intensity ratio variation between $3d$ and $4d$ peaks strongly favors a model where antimony enrichment is restricted to the topmost ionic layer (*9*). Thus we adopt this model for a more detailed interpretation of the $3d_{3/2}$ intensity ratios depicted in Fig. 7.

Suppose that a fraction θ of surface cation sites are occupied by antimony and that there is an abrupt return to bulk composition in the next atomic layer from the surface. Ignoring the (small) contribution to the photoelectron flux from antimony ions in the bulk, the intensity ratio between antimony and tin signals is then given by

$$\frac{I(\mathrm{Sb})}{I(\mathrm{Sn})} = \frac{\sigma(\mathrm{Sb}:3d)[\theta(1-\exp(-D/\lambda))]}{\sigma(\mathrm{Sn}:3d)[\exp(-D/\lambda) + (1-\theta)(1-\exp(-D/\lambda))]} \quad (11)$$

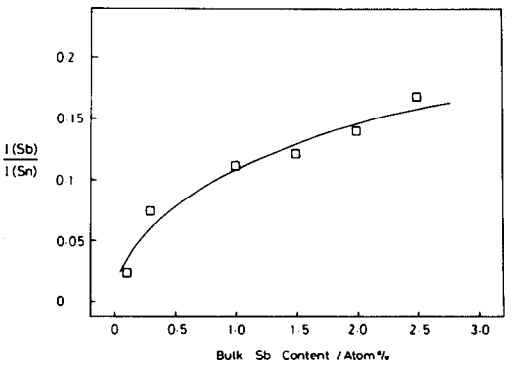

FIG. 7. Intensity ratio between Sb : $3d_{3/2}$ and Sn : $3d_{3/2}$ signals in Mg$K\alpha$ XPS of antimony-doped tin(IV) oxide. The solid line is for heuristic purposes only.

where the σ are subshell ionization cross-sections, D is the separation (normal to the surface) between adjacent cation-containing planes, and λ is the electron mean free path. Assuming that the electron scattering that leads to photoelectron attenuation can be described using a bulk jellium model for the solid, Leckey and co-workers (*21, 22*), have derived a simple expression relation the electron pathlength $\lambda(E)$ to the kinetic energy E:

$$\lambda(E) = 1.8\ \bar{E}\ E^{3/4}/E_p^2 \qquad (12)$$

In this equation all energies are in electron volts and E_p is the plasma energy characteristic of all valence electrons in the system, according to the expression:

$$E_P = 28.8\ (\rho z/A)^{1/2} \qquad (13)$$

where ρ is the density, A is the formula weight, and z is the number of valence electrons per formula unit. In (12) $\bar{E}$ is the centroid of the optical loss function which can be approximated as follows:

$$\bar{E} = E_P + E_g \qquad (14)$$

where E_g is the gap between valence and conduction bands. Assuming that O:2*p*, O:2*s*, and Sn:4*d* electrons contribute to the valence electron plasmon one has E_P = 31.6 eV and with E_g = 3.8 eV (*23*) this gives $\bar{E}$ = 35.4 eV. Through Eq. (12) we thus estimate a path length λ = 9.2 Å at the photoelectron energy appropriate to the metal 3*d* region of the spectra.

We are now in a position to use Eq. (11) to estimate surface antimony occupancy, using empirical estimates of subshell ionization cross-sections taken from the tabulation of Evans and co-workers (*24*). For a polycrystalline material there is some ambiguity in the choice of the intercationic separation normal to the surface. For simplicity we choose D to be the spacing between cation planes along the (110) direction. It then transpires that for $Sn_{0.97}Sb_{0.03}O_2$ $\theta \sim 1$, i.e., surface cation sites are exclusively occupied by antimony. For other compositions correspondingly lower surface occupancies are found.

From these data we can make very rough estimates of the heat of segregation of antimony to the surface of doped SnO_2. Simple thermodynamics (*25*) leads to the following relationship between surface (s) and bulk (b) antimony cation site occupancies:

$$\frac{\theta_s}{1-\theta_s} = \frac{\theta_b}{1-\theta_b} \exp -\frac{\Delta H}{RT} \qquad (15)$$

where ΔH is the heat of segregation and T is the temperature. In deriving the heats of segregation shown in Fig. 8 we assume that the surface is equilibrated with the bulk at 550°C, the temperature used for sample cleaning. It will be seen from Fig. 8 that the heat of segregation decreases slightly with increasing antimony content and has a limiting value of about 30 kJ/mole for the lowest concentrations. Given the various approximations involved, this estimate is in remarkably good agreement with the value of 40 kJ/mole obtained from temperature variation of the antimony XPS intensity measured by Cross and Pyke (*3*).

3.4. General Remarks

The conduction-to-valence band intensity ratio in UPS and plasmon frequency in HREELS are both consistent with a concentration of electrons in the Sn:5*s* conduction band close to the bulk value. The effective sampling depth in UPS is determined by the electron path length in the relevant kinetic energy regime and is probably in the range 5–10 Å. The penetration depth of the surface plasmon in HREELS is governed by v/ω (see Eq. (6)) and is about 50 Å using a 25-eV beam to probe a 0.5-eV excitation. In XPS we have an electron pathlength close to 10 Å and although the technique is more sensitive to details of surface structure than electronic EELS it is less sensitive than UPS. Superficially then

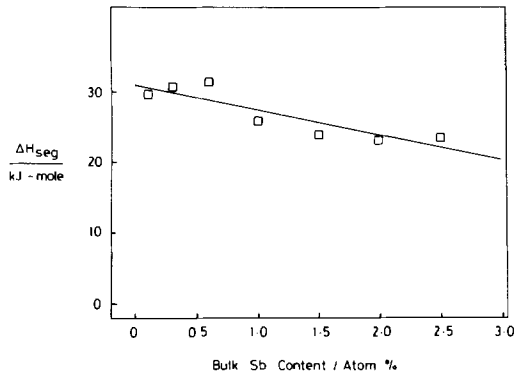

FIG. 8. Heat of segregation of antimony to surface of doped SnO_2 as a function of composition. The solid line is a heuristic least-squares fit to the experimental data.

it is difficult to reconcile the observed 10-fold surface enrichment in antimony with the low conduction electron concentration probed by UPS and EELS.

Consider a model where antimony enrichment arises from a surface "phase" thick compared with the probing depths of XPS, UPS, and EELS. Each antimony ion in regular cation rutile sites would donate one electron to the conduction band, giving a surface free-carrier concentration larger by a factor of around 10 than found experimentally. One is thus forced to conclude that this model is incorrect and that segregated antimony ions do not contribute electrons to the conduction band. Simple ionic model calculations indicate that the cation site potentials near the surface of an ionic crystal differ little from those in the bulk (*26*). In particular for the rutile lattice one expects a significant field gradient at the cation site only in the topmost ionic plane. The asymmetric environment of these genuine surface cations can lead to strong *s–p* hybridization which splits a local lone-pair like surface state off from the bulk conduction band. Thus provided antimony enrichment is restricted to the topmost cation plane, segregated Sb ions do not necessarily contribute electrons to the conduction band. Indeed one knows from the gas-phase uv photoelectron spectrum of the "model" compound Sb_4O_6 that Sb(III) lone-pair states overlap significantly with O : 2*p* states (*27*). Thus we propose that the "surface state" associated with segregated Sb ions in doped SnO_2 overlaps the O : 2*p* valence band and for this reason is not observed in ultraviolet photoelectron spectra. Note that M(III) cations may be accommodated at the surface of a material based on bulk M(IV) cations without development of a surface charge owing to flexibility in surface oxygen content.

The proposed existence of lone-pair-like surface states for antimony-doped tin(IV) oxides has clear implications with regard to the chemical behavior of such surfaces. This will be the subject of future publications.

Acknowledgments

We are grateful to Dr. P. A. Cox for a number of stimulating conversations and to Dr. W. H. Patterson who first interested us in this research. The equipment used was funded by the SERC. Thanks are due to Shell Research Ltd. for the award of a Fellowship to RGE and a CASE research studentship to PJT. X-Ray emission spectra were measured by S. Chowdhury.

References

1. W. R. PATTERSON *in* "Catalysis and Chemical Processes" (R. Pearce and W. R. Patterson, Eds.), Leonard Hill, Glasgow (1981).
2. B. GRZYBOWSKA, J. HABER, W. MARCZEWSKI, AND L. UNGIER, *J. Catal.* **42,** 327, (1976).
3. Y. CROSS AND D. R. PYKE, *J. Catal.* **58,** 61 (1979).
4. F. J. BERRY, "Advances in Catalysis," Vol. 30, p. 97, Academic Press, New York (1982).
5. F. J. BERRY AND B. J. LAUNDY, *J. Chem. Soc. Dalton* 1442 (1981).
6. D. PYKE, R. REID, AND R. J. D. TILLEY, *J. Solid State Chem.* **25,** 230 (1978).
7. D. J. SMITH, L. A. BURSILL, AND F. J. BERRY, *J. Solid State Chem.* **44,** 326 (1982).
8. P. A. COX, R. G. EGDELL, C. HARDING, A. F. ORCHARD, W. R. PATTERSON, AND P. TAVENER, *Solid State Commun.* **44,** 837 (1982).

9. P. A. Cox, R. G. Egdell, C. Harding, W. R. Patterson, and P. Tavener *Surf. Sci.* **123,** 179 (1982).
10. J. L. Jacquemin and G. Bordure, *J. Phys. Chem. Solids* **36,** 1081 (1975).
11. J. Robertson, *J. Phys. C.* **12,** 4767 (1979).
12. J. A. Marley and R. C. Dockerty, *Phys. Rev. A* **140,** 304 (1965).
13. P. P. Edwards and M. J. Sienko, *Phys. Rev. B.* **17,** 2575 (1978).
14. R. Summitt, *J. Appl. Phys.* **39,** 3762 (1968).
15. S. M. Goldberg, C. S. Fadley, and S. Kono, *J. Electron Spectrosc. Relat. Phenom.* **21,** 285 (1981).
16. P. A. Cox, R. G. Egdell, and W. R. Flavell, *Vacuum* **33,** 835 (1983).
17. A. D. Baden, P. A. Cox, R. G. Egdell, A. F. Orchard, and R. J. D. Willmer, *J. Phys. C.* **14,** L1081 (1981).
18. P. A. Cox, *Solid State Commun.* **45,** 91 (1983).
19. M. Nagasawa and S. Shionoya, *J. Phys. Soc. Jpn.* **20,** 1093 (1965).
20. L. Atkinson and P. Day, *J. Chem. Soc. (A)* 2432 (1969).
21. J. Szajman and R. C. G. Leckey, *J. Electron Spectrosc. Relat. Phenom.* **23,** 83 (1981).
22. J. Szajman, J. Leisegang, J. G. Jenkin, and R. C. G. Leckey, *J. Electron Spectrosc. Relat. Phenom.* **23,** 97 (1981).
23. Z. M. Jarzebski and J. P. Marton, *J. Electrochem. Soc.* **123,** 299C (1976).
24. S. Evans, R. G. Pritchard, and J. M. Thomas, *J. Electron Spectrosc. Relat. Phenom.* **14,** 341 (1978).
25. G. A. Somorjai, "Chemistry in Two Dimensions: Surfaces," Cornell Univ. Press, Ithaca (1981).
26. A. A. Williams and P. A. Cox, personal communication.
27. R. G. Egdell, M. H. Palmer, and R. H. Findlay, *Inorg. Chem.* **19,** 1314 (1980).